

MODELING OF A NON-PHYSICAL FISH BARRIER

Marcela Politano, Research Engineer, IIHR – Hydroscience & Engineering, The University of Iowa, Iowa City, IA, marcela-politano@uiowa.edu; Ezequiel Martin, Assist. Research Scientist, IIHR – Hydroscience & Engineering, The University of Iowa, Iowa City, IA, juan-martin@uiowa.edu; Yong Lai, Hydraulic Engineer, Technical Service Center, Bureau of Reclamation, Denver, CO, ylai@usbr.gov; Merlynn Bender, Hydraulic Engineer, Technical Service Center, Bureau of Reclamation, Denver, CO, mbender@usbr.gov; Dave Smith, Research Ecologist, US Army Corps of Engineers, Vicksburg, MS.

Abstract: Non-physical barriers (NPBs) are used to deter fish from entering an undesirable pathway without restricting flow. NPBs are commonly comprised of a bubble curtain, low-frequency sound, and hi-intensity light-emitting diode (LED) Modulated Intense Lights (MILs). In this study a 3D numerical model was developed to predict bubble, sound and light fields in the vicinity of an NPB. A Boussinesq approach was used to account for the reduction of density in the zones where bubbles are present. A simplified diffusive model for the sound intensity was developed. Two methods are proposed for light, one for high attenuation/scattering conditions based on P-N models and the other for low scattering conditions based on the superposition of analytical solutions for elementary one-dimensional cases. To validate the solvers, several experiments were simulated. A sample model application to a simplified NPB located in Georgiana Slough in the Sacramento River is presented and discussed.

INTRODUCTION

Non-physical barriers (NPBs) use behavioral stimuli such as bubbles, low-frequency sound, and high-intensity light-emitting diode (LED) Modulated Intense Lights (MILs) to deter fish from entering undesirable locations. The sound is concentrated within the bubble curtain due to the difference in the velocity of sound of water and air to prevent sound saturation. Lights projected onto the bubble curtain improve visibility for fish swimming in the direction of the curtain. This NPB arrangement is typically referred to as a Bioacoustic Fish Fence (BAFF).

The migration of juvenile salmonids in the San Joaquin and Sacramento Rivers is of great environmental interest due to decline of native species. Fish diversion into the Delta may result in delayed migration, elevated risk of predation, exposure to poor water quality conditions, and mortality in pumping facilities. The California Department of Water Resources (CDWR) and the U.S. Bureau of Reclamation (Reclamation) proposed to use a NPB to reduce the diversion of juvenile salmonids from the Sacramento River into the interior and south Delta. The effectiveness of NPBs in deterring fish is variable, depending on the location, barrier geometry, and river flows. NPB can also have unintended effects, such as increased predation upstream and downstream of the barrier. All the above increase the environmental risk requiring site specific study and evaluation. In this study a numerical model for a NPB was developed to better understand the effect of the barrier on the Sacramento River hydrodynamics and support the design and operation of a NPB to deter and direct fish movement.

NUMERICAL MODEL

In this study, we first developed the model equations to simulate the bubbles, sound and light fields. The model equations were then implemented into the open source code OpenFoam (Weller et al. 1998). OpenFoam is a collection of C++ libraries, based on object oriented programming, designed for continuum mechanics applications. A new solver, pisoFoamBLS, which includes simplified models for predicting bubbles, sound and light fields near a non-physical fish barrier, was developed based on the code pisoFoam using a modular approach. Several studies related to implementation of different solvers in OpenFoam may be found in the literature (Hussein 2009, Kassem et al. 2011, Flores et al. 2013, among others) and repeated herein.

MODELING OF BUBBLES

Mathematical Modeling

A bubbly flow, i.e., a discrete gas phase in a continuous fluid, is formed in bubble curtains. As illustrated in Figure 2, bubbles injected in an initially quiescent medium induce a motion in the liquid similar to that observed in buoyancy-induced flows. Three distinct zones can be observed in a bubble curtain:

1. The primary bubble zone: where bubbles accelerate as they detach from the nozzle

2. The plume zone: where bubble breakup and coalescence prevail to form the plume
3. The free bubble zone: where the dynamic process of breakup and coalescence have reached an equilibrium and bubbles rise without significant size change

Measurements of gas volume fraction, bubble frequency and chord length by Castillejos and Brimacombe (1987) indicate that bubble breakup in the plume zone predominantly occurs near the injection location. Close to the free surface, the bubble velocity decreases as liquid moves tangent to the free surface, which enhances coalescence and promotes larger bubble sizes.

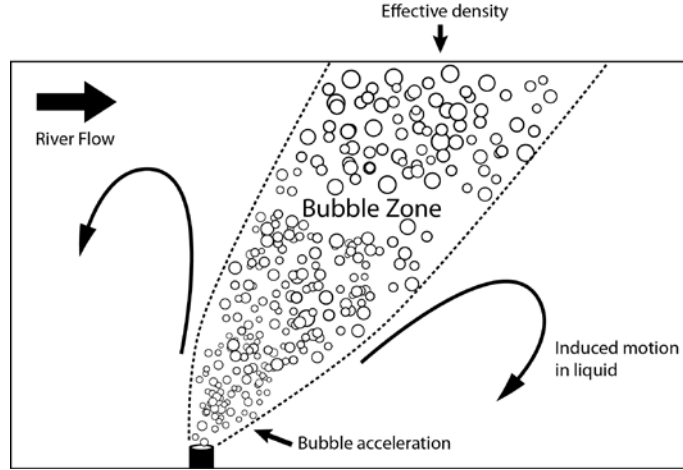


Figure 1. Induced liquid motion for a bubble curtain in a river

Most of bubble plume models found in the literature are intended for the free bubble zone region. The current modeling effort is based on the model presented by Buscaglia et al. (2002). The authors used a two-fluid approach assuming an incompressible mixture gas-liquid phase. In this approach, the Navier-Stokes equations are restored, significantly simplifying the formulation. The main advantage of this model is that an equation for the gas phase is included and therefore the shape of the bubble zone can be predicted. Future model improvements such as inclusion of a bubble size distribution, breakup and coalescence, bubble dissolution, bubble compression, bubble induced turbulence, etc., can easily be incorporated into the model using this formulation. Following Buscaglia et al. (2002), density differences are neglected except where they appear in the term multiplied by the acceleration due to gravity resulting in:

$$\nabla \cdot \vec{u}_m = 0 \quad (1)$$

$$\rho_l \frac{\partial}{\partial t} \vec{u}_m + \rho_l \nabla \cdot (\vec{u}_m \vec{u}_m) = -\nabla P + \nabla \cdot [\tau_m^{Re} + \tau_m] + \rho_m \vec{g} \quad (2)$$

Eqs. (1) and (2) can be solved to compute pressure and velocity of the mixture phase with any single-phase CFD solver adding a source term in the momentum equation $\vec{S}_m = -(\rho_l - \rho_g) \alpha \vec{g}$. In this study an isotropic turbulence model $k - \varepsilon$ was used for turbulence closure. The gas velocity was obtained from the momentum equation for the gas phase. Inertia, gravity force and viscous shear stresses are significantly smaller than liquid-gas interfacial forces due to the small density and viscosity of the gas phase and are usually neglected. In this particular application, drag is the most important interfacial force and lift and virtual mass can be neglected resulting in:

$$-\nabla \left(P + \frac{2}{3} k \right) + \frac{3}{8} \frac{C_g^D}{R} \vec{u}_r |\vec{u}_r| = 0 \quad (3)$$

In a bubble curtain, bubble size can change due to breakup, coalescence, mass transfer and pressure variations. In this study, an equation for the bubble number density was used:

$$\frac{\partial N}{\partial t} + \nabla \cdot [\vec{u}_g N] = \frac{v'}{Sc} \nabla^2 N_g \quad (4)$$

The bubble volume at a given position can be calculated from $v_b = \frac{P_c}{P} \frac{4}{3} \pi R_c^3$, where P_c and R_c are the pressure and radius at the injection point. The bubble zone can be determined using the gas volume fraction, which can be obtained from the mass conservation equation for the gas phase $\alpha = \frac{4}{3} \pi R^3 N$.

Model Comparison with Experiments

The model was used to simulate an experiment by Grevet et al. (1982) in which a water-filled cylindrical tank was agitated by a gas bubble stream, and compared against velocity data measured inside the tank. The modeled tank radius, R , was 0.3 m and the water height, H , 0.6 m. Bubbles were injected into the quiescent liquid through an orifice of 0.0127 m (0.5 inch) at a flowrate of 205 cm³/s. Only one fourth of the tank was simulated to reduce grid size and computational time. Symmetry boundary conditions were used on the sides. Grid size was approximately 10⁵ nodes. Since bubble velocities were not measured, it is assumed that bubbles enter the domain at their terminal velocity. Reasonable agreement was found between model predictions and experimental data for three axial positions (Figure 2). As rising bubbles leave the injector, they generate an inward flow at the left bottom side of the tank. The bubble stream then generates an upward flow in the center of the tank and a large clockwise vortical structure at the upper right side, with negligible radial velocities. The rising bubble velocity is terminated at the free surface and the liquid vertical moment is converted to horizontal flow. The horizontal flow is blocked by the tank wall and is redirected downward along the side wall. The model is considerably less accurate near the walls, but since wall interaction is not important in a bubble curtain, grid refinement was not performed to capture the velocity profile near the walls. The proposed model assumes one variable bubble size. Implementation of a bubble size distribution is expected to improve model accuracy. Figure 3 shows the gas volume fraction distribution in the tank. For the low gas volume fraction injected, bubbles concentrated in the core of the tank, rise almost uniformly in a nearly straight line. Near the injector, bubble velocity increases due to the upward liquid flow in the center of the tank. This local increase of the liquid velocity causes a reduction of the gas volume fraction. Conversely, bubble velocities are reduced near the free surface resulting in a local increase of the gas volume fraction.

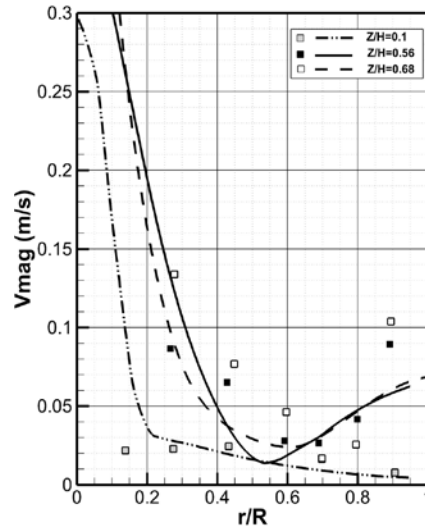


Figure 2. Comparison between predicted and measured velocity magnitude. Symbols: experiments by Grevet et al. (1982) and lines: model results

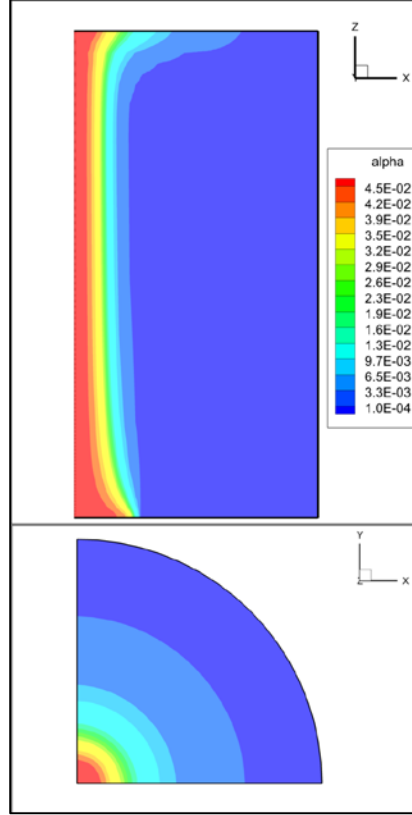


Figure 3. Gas volume fraction contours

MODELING OF SOUND

Mathematical Modeling

The acoustic field in a domain can be represented by an equation of acoustic energy conservation:

$$\frac{\partial W}{\partial t} = -\nabla \cdot \mathbf{I} - D \quad (5)$$

where W is the acoustic energy and \mathbf{I} the acoustic energy flux. The last term in the RHS represents dissipation effects. In this study a method was developed to deal with the strong changes in fluid properties introduced by the presence of the bubble barrier as well as the multiple surfaces that partially absorb the sound signals at the boundaries. The diffusive equation used in architectural acoustics was identified as a viable candidate to fulfill these requirements. A Fick's law-type relation is postulated between the energy flux and the energy density, $\mathbf{I} = -\mathbf{D}_W \nabla W$, which adapted to give a dependence of the dissipation on W rather than \mathbf{I} , transforms the conservation equation for sound energy to:

$$\frac{\partial W}{\partial t} = -\nabla \cdot (\mathbf{D}_W \nabla W) - \alpha_W^2 |\mathbf{D}_W| W + S_W \quad (6)$$

where a general distributed source term S_W has also been included. A new parameter, an anisotropic diffusion coefficient \mathbf{D}_W , has been introduced, for which modeling is required. The expression for the dissipation term is such that the exponential decay of a plane wave in an isotropic media is recovered. Following Picaut (2002), absorption is modeled as a boundary condition. Picaut et al. (1999) proposed a diagonal tensor related to length-scale of domain for the diffusion coefficient:

$$\frac{D_{xx}}{\ell_x} = \frac{D_{yy}}{\ell_y} = \frac{D_{zz}}{\ell_z} = D_{3D} \quad (7)$$

with the diffusion proportional to sound speed ($D_{3D} \sim c$). Eq. (6) is a standard diffusion equation for which solution methods are well established and can be readily implemented in OpenFoam. Certain features of the sound field are lost by using this approach, such as the appearance of interference patterns and the rapid evolution of the sound field that can be found with the ray tracing method. However, it is questionable that those features are of significant importance for the current application, as it is expected that the cases of interest will be quasi-steady in both bubble-encapsulated and non-encapsulated sound fields as the fluid velocity is much smaller than the speed of sound, and the sound source are non-pulsating in time.

A set of linear attenuation coefficients and speed of sound data for bubbly flows presented by Silberman (1957) were used in this study.

Model Comparison with Experiments

The data presented by Würsig et al. (2000) represent one of the few reported field experiments with useful, albeit scarce, data for model validation. Sound levels produced by a pile-driving hammer in shallow waters were measured with and without a bubble curtain designed to mitigate the sound. Measurements of background noise are also available, but there is no measurement of sound levels near the source or inside the bubble curtain area. A slab geometry with an average depth of 8 meters was simulated. In Figure 4, the measured data on April 26, 1996 is shown along with the simulated results. The authors reported an overall sound level for frequencies spanning 100 Hz to 25.6 kHz, as well as results for the different one-octave bands. Notable differences in attenuation by the bubble curtain occur for the different frequencies, but it was found that the reported average trend for all frequencies is consistent with the results for low frequencies (as the sound intensity is largest for the 400 Hz octaves), and a representative frequency of 400Hz was chosen to perform the simulations. A uniform source for the background noise and an additional source near the coordinates' origin were obtained. The relationship between the wall attenuation coefficient and the diffusion parameter was established using the expression proposed by Silberman (1957). An extremely low value of $D_{yy} / D_{rr} = 1.6 \times 10^{-4}$ was found from the experimental data, and as shown in Figure 4, the predicted decay matches well with the data. Finally, a mean gas volume fraction was estimated from the reported flow rate, assuming a terminal bubble velocity and a corresponding plume spreading angle. The resulting bubbly region is a ring, 25 m in diameter and 0.5 meter in thickness, with an estimated gas volume fraction of 0.02. It is reported that the resulting attenuation by the bubble barrier is about 3 to 5 dB, which agrees well with the estimated attenuation. The simulations required a smaller value of gas volume fraction to match the data of 0.003. When experimental data become available, further simulations and analyses should be performed to identify the reason for this discrepancy.

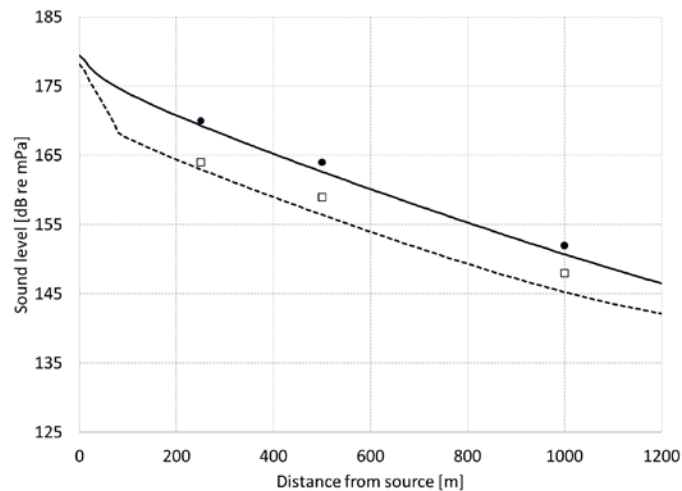


Figure 4. Sound levels in a slab. Symbols: Würsig et al. (2000) experimental data (black circles: bubble curtain off; white squares: bubble curtain on) and lines: simulation results

MODELING OF LIGHT

Mathematical Modeling

Calculations of light intensity can be extremely resource-intensive and are typically done using Monte Carlo simulations; or are based on semi-analytical approximations to an integro-differential equation. The latter approach was used in this study. The fundamental equation describing the light field in a continuous media is called the radiative transfer (RT) equation. The RT conservation equation balances the changes of spectral radiance (L) in a given direction with the processes that can modify it: *absorption*, *scattering* and *emission*. The attenuation of the beam is given by the *absorption*, defined by the absorption coefficient $a_E(\mathbf{x}, \lambda)$ times the radiance and all the scattering *out* of the beam direction that can be approximated as $-b_E(\mathbf{x}, \lambda)L$, with b_E the average of the volume scattering function. The elastic (i.e., without a change of wavelength) *scattering* for other directions *into* a given direction constitutes a source and is represented as an integral that accounts for all the contributions over all possible 4π solid angle directions to a given one. Finally, *emission* may correspond to an actual source or due to inelastic scattering from other wavelengths, and can be expressed as a general source s_E , per steradian. The complete RT equation can be written as (Mobley, 2001):

$$\Omega \nabla L(\mathbf{x}, \theta, \varphi, \lambda) = -c_E(\mathbf{x}, \lambda)L(\mathbf{x}, \theta, \varphi, \lambda) + \int_{4\pi} L(\mathbf{x}, \theta', \varphi', \lambda) \beta_s(\mathbf{x}, \theta', \varphi', \theta, \varphi, \lambda) d\Omega' + s_E(\mathbf{x}, \theta, \varphi, \lambda) \quad (8)$$

with β_s is the angle dependent volume scattering function and c_E the sum of a_E and b_E . Eq. (8) contains both an integral on the solid angle and spatial derivatives which can be very difficult to solve explicitly. In this study, the scalar irradiance, E , obtained by integration of L , was used. Extensive literature exists on different methods implemented to solve Eq. (8). In this study, two methods were implemented. A superposition of elementary solutions is proposed when scattering effects are not important and a P-1 model for high attenuation and/or scattering.

Certain apparent optical properties such as the diffuse attenuation coefficient can be approximated as a function of intrinsic properties for certain simple cases (Kirk, 2003; Kirk, 2006). Two simple solutions for the scalar irradiance can be found for planar and point sources by simple integration of Eq. (10):

$$E(z) = E_0 \exp(-Kz) \quad (9)$$

$$E(r) = \frac{r_0^2}{r^2} E_0 \exp(-Kr) \quad (10)$$

In the superposition of elementary solutions method, multiple elementary solutions are automatically combined to produce a light field that approximates the solution of RTE:

$$\nabla \cdot (\mathbf{u}_E E) = S_E - KE \quad (11)$$

where $S_E = 4\pi s_E$, and K is the diffuse attenuation coefficient. To recover the solutions presented before (Eqs. 9 and 10), a dimensionless vector field is defined as $\mathbf{u}_E = (0, 0, -1)$ for a plane source emitting in the z negative direction and $\mathbf{u}_E = \mathbf{e}_r$ the radial unit vector for the point source case. By presenting the solution as a result of a numerical integration it is possible to introduce more complex geometries and also variability of the attenuation factor, which can be calculated independently of the solution. With this simple scheme it is possible to reproduce background illumination due to natural daylight as a plane source, as well as including the stroboscopic lights of the barrier as point sources.

P-N models use a diffusive representation of the RTE, and as such its range of validity is for conditions with high attenuation and/or scattering (Sazhin et al., 1996). In general, P-N models are based on the expansion of the solution to RTE in orthogonal series of spherical harmonics. For the P-1 model only the first and third terms of the series are kept resulting in:

$$-\sum_{i=1}^3 \frac{\partial}{\partial x_i} \frac{1}{3(a_E + b_E)} \frac{\partial L^{(0)}}{\partial x_i} = 4\pi s_E - a_E L^{(0)} \quad (12)$$

Attenuation and absorption coefficients available in USEPA (2000) and Mobley (2001) as a function of water molecules, chlorophyll, inorganic matter and colored dissolved organic matter were used.

For a bubbly flow, the effect of the bubbles in the attenuation of light must also be considered. For most cases, it can be assumed that the bubble's radius R is much larger than the wavelength of the incident light. This condition is known as the geometric optic limit, for which both the geometric approximation and the Mie theory of scattering will predict the same far-field solution for the interaction of a plane wave and a single large sphere (Randrianalisoa and Baillis, 2014). It is a good assumption to neglect the absorption within the bubble and only consider the scattering contribution (Shamoun et al., 1999). For multiple scatters, the interaction between particles can be neglected if the characteristic spacing between particles is large compared to both the wavelength and the particle radius. In that case, the scattering characteristics can be obtained as a summation of the individual contributions. The resulting extinction coefficient due to bubbles is $c_b = \frac{3\alpha}{4R}$.

In this study reflections at the boundaries from the original sources were implemented using a cosine emission law.

Model validation

Some simple geometries were run to validate the implemented models and to highlight the differences between the two models. Unfortunately, no data for controlled bubbly flows were identified that could be simulated, other than some information on attenuation coefficients that was already included in the modelling process.

The dimensionless irradiance field for two point sources in a closed cavity were simulated. First reflections are possible in the bottom boundary only. The model predicts the irradiance reduction with the radial distance shown in Eq. (10) (Figure 5). Total irradiance shown on the left frames is the summation of incidente (middle frame) and reflected (right frame) irradiances. This case shows the feasibility of representing the modulated intense lights (MILs) for the fish barrier as the solution of superimposed single point sources.

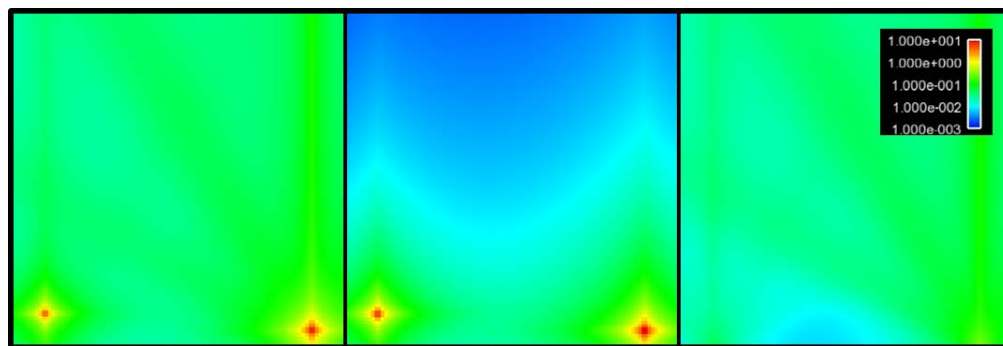


Figure 5: Total irradiance (left), incidente (middle) and reflected (right) from two point sources near the bottom of a cavity

The focus of the validation of the P-1 model was to demonstrate the effect of bubbles on the distribution of the irradiance. Figure 6 shows the basic profile for the case where no bubbles are present. As expected, the irradiance decays radially from the source with an equivalent diffuse attenuation coefficient $K = (3a_E c_E)^{1/2}$. Two possible boundary conditions are shown in Figure 6 for the boundary closest to the source, the partial reflective condition (left frame) and full reflective conditions (right frame). As expected, the latter results in larger values for E , but given the rapid decay of the irradiance most differences between the two cases are localized to the region immediate to the source and very close to the boundary.

The deformation of the radial pattern due to the presence of a bubble curtain is shown in Figure 7. The extension of the curtain is shown with dashed lines. Several values of gas volume fraction with fully reflecting boundary were considered. The main effect of the bubbles is to concentrate the light field into a smaller region and with a larger maximum value for E . The distribution of the light field varies radically depending on whether the light source is contained in the bubble curtain, in which case very little illumination escapes the curtain, or whether the source is placed near the curtain, in which case bubbles act as a reflector.

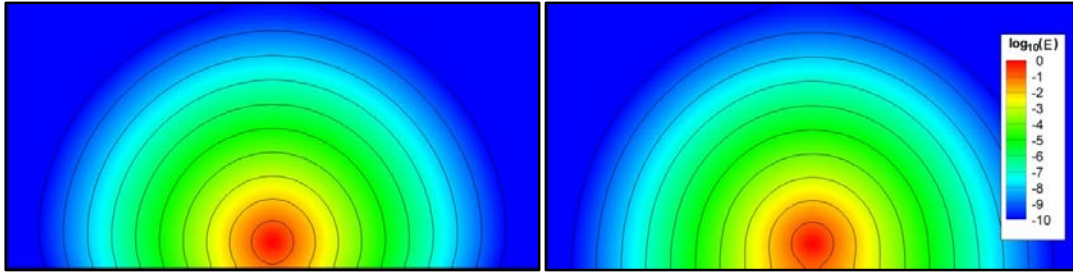


Figure 6. Unit irradiance source near a boundary. Left, lower boundary correspond to a water-air interface; right, fully reflecting boundary

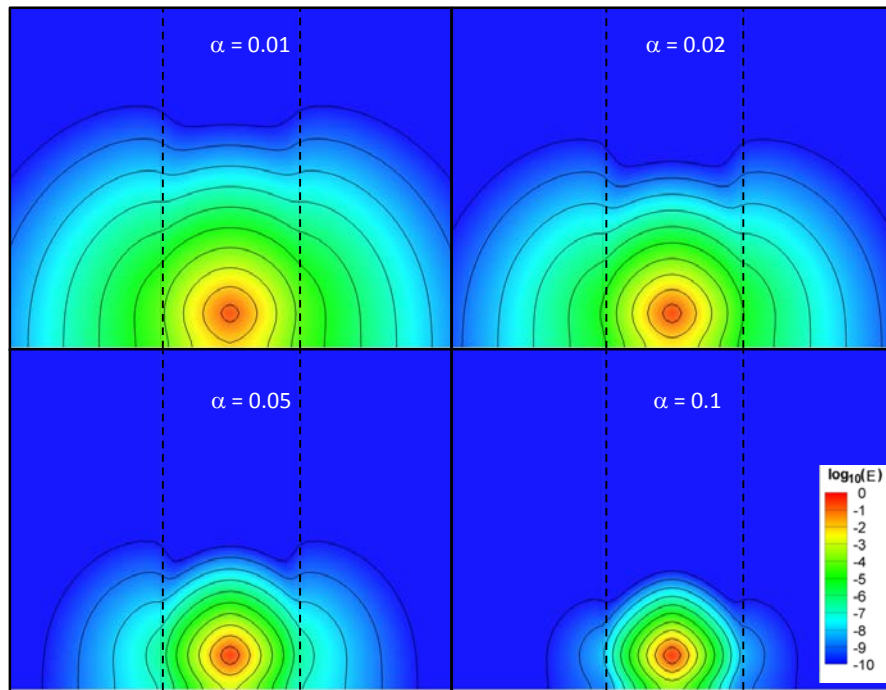


Figure 7: Unit irradiance source within a bubble curtain near a boundary

SIMULATION OF A NON-PHYSICAL FISH BARRIER

Simplified Georgiana Slough

A main channel with two bifurcations and a non-physical fish barrier upstream of the smallest stream was simulated to test the capability of the proposed model to predict the flow field and bubble, sound and light fields in the vicinity of a fish barrier (Figure 8). The geometry of the Georgiana Slough in the Sacramento River was used (McQuirk and Reeves, 2012). Since bathymetric information was not available a constant water depth of 9.1 m was used. This value was selected based on information of underwater sound measurements that were taken between 2.9 m to 14.6 m (McQuirk and Reeves 2012). In this paper a simulation using typical conditions in the Sacramento River upstream of the Georgiana Slough is presented. Flowrates upstream and downstream of the curtain were $334 \text{ m}^3/\text{s}$ and $132 \text{ m}^3/\text{s}$, respectively. Small bubbles of 0.8 mm (0.03 inch) diameter were injected at the bottom of the river at a pressure of $1.91 \cdot 10^5 \text{ Pa}$ and at $25 \text{ }^\circ\text{C}$. The diffusion coefficient was set using Eq. (12), with constant $D_{3D} = 0.1c_{\text{water}}$, $l_z = 10 \text{ m}$ and $l_x = l_y = 200 \text{ m}$, a mixed boundary condition was imposed on the bottom and the side walls, and release conditions at the surface. Sound sources operating in the range 5-600 Hz with a mean sound level of 152 dB re $1 \mu\text{Pa}$ were installed in the field near Georgiana Slough (McQuirk and Reeves, 2012). A far field value ($\sim 200 \text{ m}$) of about 110 dB re $1 \mu\text{Pa}$ was reported. In this study, nineteen sound projectors were located immediately downstream of the bubble barrier and

each projector was modeled as a constant source of acoustic energy density of 0.01 W/m. Four light sources of 10 W/m³ were included upstream of the bubble barrier.

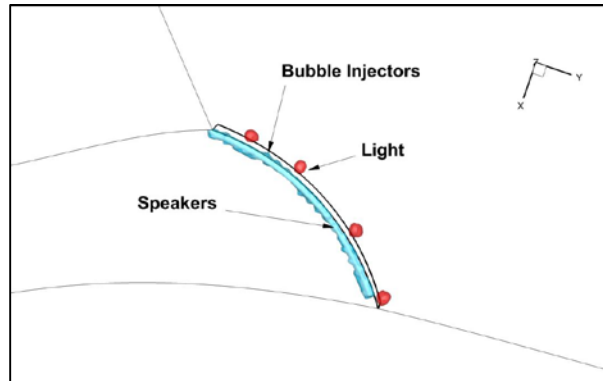


Figure 8. Simulated fish barrier

Figure 9 shows slices near the river bed (a), in the mid plane (b) and at the free surface (c). Vectors were interpolated in an equally-spaced structured mesh to enhance visualization. Bubbles significantly modify the flow pattern near the curtain. Two phenomena affect the gas volume fraction distribution; the most important is the buoyancy that drives bubbles toward the free surface and the other is the downstream convective transport by the river. The latter is significant at high river velocities and can be noted downstream of the curtain where the plume is directed towards the left bank. Upstream of the curtain and at small depths, the liquid velocity reverses direction due to the horizontal surface flow created when the plume reaches the free surface.

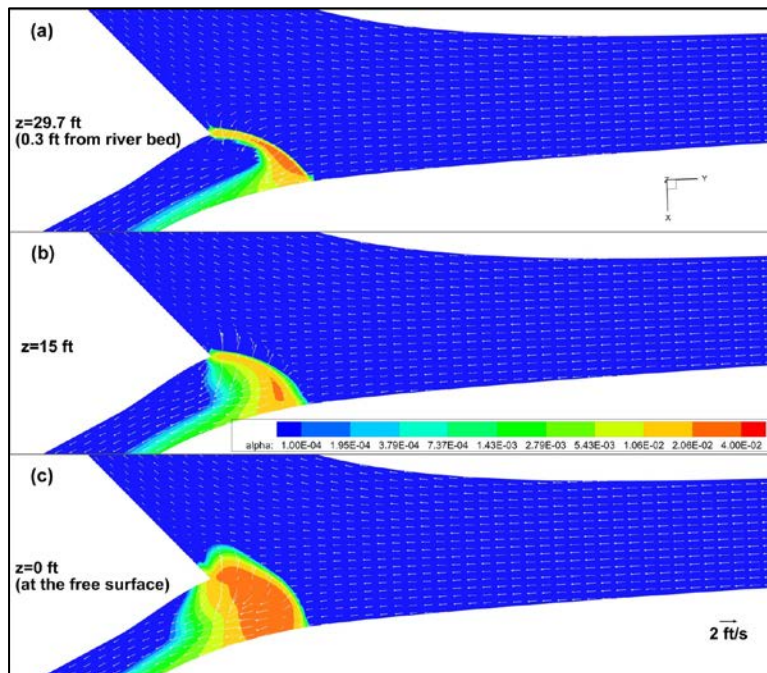


Figure 9. Gas volume fraction and velocity vectors at (a) 9 m (29.7 ft), (b) 4.5 m (15 ft) and (c) 0 m (0 ft)

Figure 10 shows flow characteristics near the bubble curtain. The frames in the top and middle show gas volume fraction isosurfaces and distribution of gas volume fraction at slices through the middle of the channels, respectively. Bubbles are transported away from the plume center by the strong surface current induced by the gas phase. The gas distribution and flow pattern are not symmetric relative to the bubble plume center due to the geometry and convective

transport by the river flow. Streamlines colored by velocity magnitude in the bottom frame show back flow near the inner wall of the larger branch towards the bubble curtain.

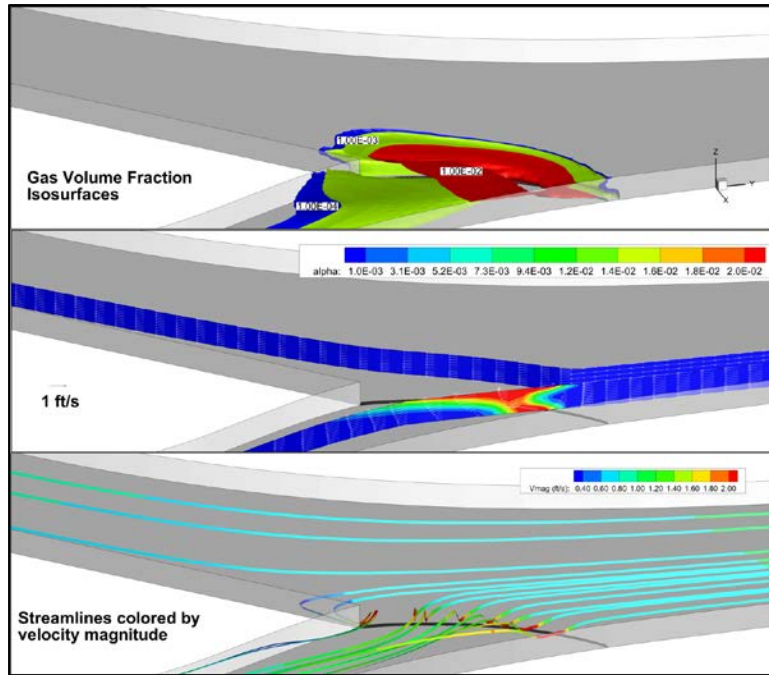


Figure 10. Gas volume fraction isosurfaces (top), gas volume fraction distribution in each river branch (middle), and streamlines colored by velocity magnitude (bottom)

Figure 11 shows the gas distribution and recirculation zones generated by the bubble curtain. As the bubble plume rises through the water column it entrains ambient water inducing two recirculating zones. Near the injector, the gas volume fraction is reduced as bubble velocity increases due to entrained liquid into the plume. On the other hand, near the free surface, the gas volume fraction increases for two phenomena, one is the increment in bubble volume due to decompression and the other is the reduction of liquid vertical velocity near the free surface. Note that since slip velocity increases with bubble size, a larger relative velocity is expected near the free surface. However, this effect is less important than the reduction of liquid velocity by the free surface.

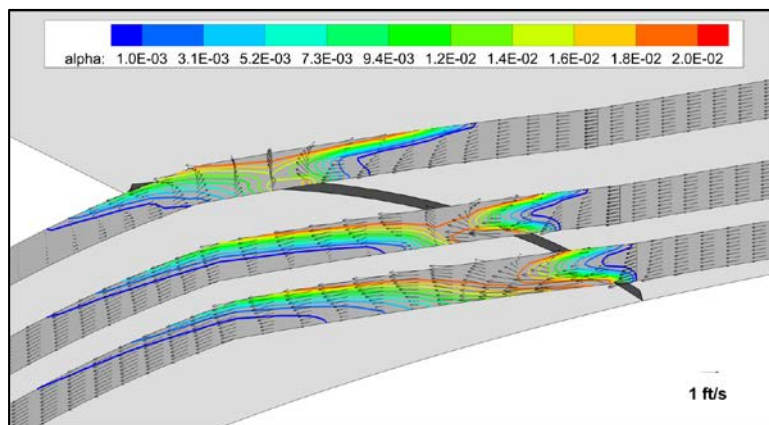


Figure 11. Gas volume fraction and velocity vectors near the bubble curtain

Figure 12 shows isosurfaces of sound energy. Bubbles encapsulate the sound within the fish barrier. However, some differences in the level of sound are observed due to increased sound attenuation by bubbles transported near the outer wall along the smaller channel.

Figure 13 shows the irradiance generated by the high-intensity LED MILs predicted with the superposition of elementary solution method (a) and P1 model (b). Light scattering and absorption by the bubbles results in an appreciable concentration of light within the fish barrier.

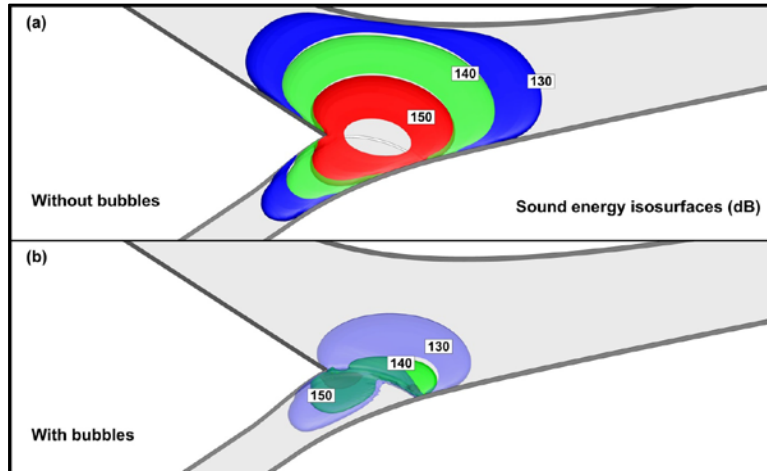


Figure 12. Isosurfaces of sound energy. Before bubble injection (a) and with bubble curtain (b)

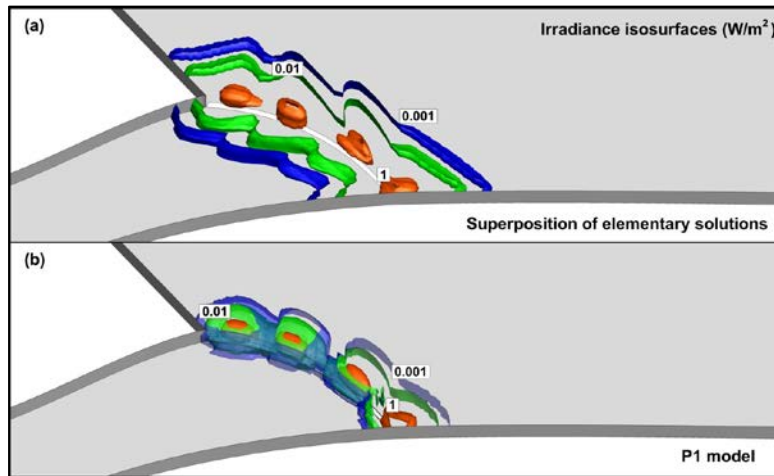


Figure 13. Isosurfaces of irradiance. Before bubble injection (a) and model P-1 with bubble curtain (b)

CONCLUSIONS AND FUTURE DIRECTIONS

Numerical models for predicting the hydrodynamics, bubble, sound, and light distributions near a non-physical fish barrier were developed. The models were implemented using a modular approach in the open source code openFoam. A Boussinesq approach was used to account for the reduction of density in the zones where bubbles are present. The effect of the bubbles on the sound and light fields were considered through attenuation coefficient models found in the literature. Simple geometries were simulated to validate the implementation of the models. Model results for a non-physical fish barrier located in a bifurcation similar to Georgiana Slough indicate that the bubble plume has a strong effect on the flow pattern near the barrier. The resulting large-scale recirculations and increased accelerations near the barrier are expected to influence fish migration route. Sound and light are strongly coupled with the bubble plume. Bubbles effectively encapsulate both sound and light within the barrier region. According to the model, the effectiveness of bubbles to attenuate sound depends on the position of the speakers relative to the bubble plume. Since

the bubble plume location depends on the induced liquid movement as well as downstream transport by the river, optimal location of speakers is a function of the river flowrate and gas injection rate through the diffusers. Additional research needs to include a full set of experimental data and monitoring near a fish barrier, at several river and barrier operational conditions, for better quantification of important variables. Examples include measurements of gas volume fraction, bubble size, river depth, liquid velocities, and sound and light fields. The complex three-dimensional nature of the problem will require measurement stations at several transects near the barrier. This is essential to fully validate and improve the developed numerical tool and identify areas where future modeling effort should focus.

REFERENCES

- Buscaglia, G.C., Bombardelli F.A. and Garcia, M.H. (2002). "Numerical modeling of large-scale bubble plumes accounting for mass transfer effects". *Int. J. Multiphase Flow*, 28, pp 1763-1785.
- Castillejos, A.H. and Brimacombe, J.K. (1987). "Measurement of physical characteristics of bubbles in gas-liquid plumes: Part II. local properties of turbulent air-water plumes in vertically injected jets". *Metallurgical Transactions B*, 18B, pp 659-671.
- Flores, F., Garreaud, R. and Muñoz, R. (2013). "CFD simulations of turbulent buoyant atmospheric flows over complex geometry: solver development in OpenFoam". *Computers and Fluids*, 82, pp 1-13.
- Grevet, J.H., Szekely, J. and El-Kaddah, N. (1982). "An experimental and theoretical study of gas bubble driven circulation systems". *Int. Journal of Heat Mass Transfer*, 25(4), pp 487-497.
- Hussein, A.S. and El-Shishiny, H. (2009). "Influences of wind flow over heritage sites: a case study of the wind environment over the Giza Plateau in Egypt". *Environ Modell Software*, 24, 389–410.
- Kassem, H., Saqr, K., Aly, H.S., Sies, M.M. and Wahid, M. (2011). "Implementation of the eddy dissipation model for turbulent non-premixed combustion in OpenFOAM". *Int. Communications in Heat and Mass Transfer*, 38, pp 363-367.
- Kirk, J.T.O. (2003). "The vertical attenuation of irradiance as a function of the optical properties of the water". *Limnol. Oceanogr.*, 48, pp 9–17.
- Kirk, J.T.O. (2006). "Light field around a point light source in the ocean". *Journal of Geophys. Res.*, 111, C07008.
- McQuirk, J. and Reeves, R. (2012). "2011 Georgiana Slough Non-Physical Barrier performance evaluation project report". California Department of Water Resources, Sacramento, CA.
- Mobley, C.D. (2001). "Radiative transfer in the ocean". in *Encyclopedia of Ocean Sciences*, edited by J. H. Steele, S. Thorpe, and K. Turekian, pp. 2321–2330, Elsevier, New York.
- Picaut, J., Hardy, J. and Simon, L. (1999). "Sound propagation in urban areas: a periodic disposition of buildings". *Physical Review E*, 60, pp 4851-4859.
- Picaut J. (2002). "Numerical modeling of urban sound fields by a diffusion process". *Applied Acoustics*, 63, pp 965-991.
- Randrianalisoa, J. and Baillis, D. (2014). "Analytical model of radiative properties of packed beds and dispersed media". *Int. J. of Heat and Mass Transfer*, 70, pp 264-275.
- Sazhin, S.S., Sazhina, E.M., Faltsi-Saravelou, O. and Wild P. (1996). "The P-1 model for thermal radiation transfer: advantages and limitations". *Fuel*, 75, pp 289-294.
- Shamoun, B., Beshbeeshy, M.E. and Bonazza, R. (1999). "Light extinction technique for void fraction measurements in bubbly flow". *Exp. in Fluids*, 26, pp 16-26
- Silberman E. (1957). "Sound velocity and attenuation in bubbly mixtures measured in standing wave tubes". *The Journal of the Acoustical Society of America*, 29, pp 925-933.
- USEPA (2000). "Chesapeake Bay submerged aquatic vegetation water quality and habitat-based requirements and restoration targets: a second technical synthesis". <http://archive.chesapeakebay.net/pubs/sav/savreport.pdf>.
- Weller, H., Tabor, G., Jasak, H. and Fureby, C. (1998). "A tensorial approach to computational continuum mechanics using object-oriented techniques". *Comp. Phys.* 12(6), pp 620–31.
- Würsig, B., Greene, C.R. and Jefferson, T.A. (2000). "Development of an air bubble curtain to reduce underwater noise of percussive piling". *Marine Environmental Research*, 49, pp 79-93.